

Precise observations of the $^{12}\text{C}/^{13}\text{C}$ ratios of HC_3N in the low-mass star-forming region L1527

Accepted 2016 October 9

MITSUNORI ARAKI^{1,2}, SHURO TAKANO³, NAMI SAKAI⁴, SATOSHI YAMAMOTO⁵, TAKAHIRO OYAMA¹, NOBUHIKO KUZE⁶, AND KOICHI TSUKIYAMA^{1,2}

¹ Department of Chemistry, Faculty of Science Division I, Tokyo University of Science, 1-3 Kagurazaka, Shinjuku-ku, Tokyo 162-8601, Japan; araki@rs.kagu.tus.ac.jp

² IR Free Electron Laser Research Center, Research Institute for Science and Technology (RIST), Tokyo University of Science, 2641, Yamazaki, Noda, Chiba 278-8510, Japan

³ Department of Physics, General Studies, College of Engineering, Nihon University, 1 Nakagawara, Tokusada, Tamuramachi, Koriyama, Fukushima 963-8642, Japan

⁴ The Institute of Physical and Chemical Research (RIKEN), 2-1 Hirosawa, Wako, Saitama 351-0198, Japan

⁵ Department of Physics and Research Center for the Early Universe, The University of Tokyo, Bunkyo-ku, Tokyo 113-0033, Japan

⁶ Department of Materials and Life Sciences, Faculty of Science and Technology, Sophia University, 7-1 Kioi-cho, Chiyoda-ku, Tokyo 102-8554, Japan

ABSTRACT

Using the Green Bank 100 m telescope and the Nobeyama 45 m telescope, we have observed the rotational emission lines of the three ^{13}C isotopic species of HC_3N in the 3 and 7 mm bands toward the low-mass star-forming region L1527 in order to explore their anomalous $^{12}\text{C}/^{13}\text{C}$ ratios. The column densities of the ^{13}C isotopic species are derived from the intensities of the $J = 5-4$ lines observed at high signal-to-noise ratios. The abundance ratios are determined to be $1.00:1.01 \pm 0.02:1.35 \pm 0.03:86.4 \pm 1.6$ for $[\text{H}^{13}\text{CCCN}]:[\text{HC}^{13}\text{CCN}]:[\text{HCC}^{13}\text{CN}]:[\text{HCCCN}]$, where the errors represent one standard deviation. The ratios are very similar to those reported for the starless cloud, Taurus Molecular Cloud-1 Cyanopolyne Peak (TMC-1 CP). These ratios cannot be explained by thermal equilibrium, but likely reflect the production pathways of this molecule. We have shown the equality of the abundances of H^{13}CCCN and HC^{13}CCN at a high-confidence level, which supports the production pathways of HC_3N via C_2H_2 and C_2H_2^+ . The average $^{12}\text{C}/^{13}\text{C}$ ratio for HC_3N is 77 ± 4 , which may be only slightly higher than the elemental $^{12}\text{C}/^{13}\text{C}$ ratio. Dilution of the ^{13}C isotope in HC_3N is not as significant as that in CCH or $c\text{-C}_3\text{H}_2$. We have also simultaneously observed the DCCCN and HCCC ^{15}N lines and derived the isotope ratios: $[\text{DCCCN}]/[\text{HCCCN}] = 0.0370 \pm 0.0007$ and $[\text{HCCCN}]/[\text{HCCC}^{15}\text{N}] = 338 \pm 12$.

Subject Keywords: Astrochemistry—ISM: clouds—ISM: molecules—ISM: individual (L1527)—Radio lines: ISM

1. INTRODUCTION

Carbon-chain molecules constitute 40% of the molecular species detected in interstellar space. They are known to be abundant in cold starless cores in early chemical evolutionary stages (Suzuki et al. 1992). Using this chemical behavior, carbon-chain molecules have been extensively employed as good tracers of the early phase of prestellar core evolution (Benson et al. 1998; Aikawa et al. 2001; Rathborne et al. 2008; Hirota et al. 2009; Marka et al. 2012). Carbon-chain molecules are also known to be abundant in a dense and warm region of some low-mass protostellar cores. This is called “warm carbon-chain chemistry (WCCC),” and its prototypical source is L1527 in Taurus (e.g., Sakai et al. 2008, 2009a; Sakai & Yamamoto 2013).

General features of the two types of carbon-chain chemistry are successfully explained by chemical models (e.g., Aikawa et al. 2001, 2008; Hassel et al. 2008). However, production pathways of individual molecular species are often controversial and are still subject to detailed investigation. For instance, the various $^{12}\text{C}/^{13}\text{C}$ ratios for nonequivalent carbon atoms constituting a carbon-chain molecule have posed an important problem in astrochemistry. Anomalies in the $^{12}\text{C}/^{13}\text{C}$ ratio are reported for HC_3N (Takano et al. 1998, Li et al. 2016, Taniguchi et al. 2016a), CCS (Sakai et al. 2007), CCH (Saleck et al. 1994, Sakai et al. 2010b), C_3S (Sakai et al. 2013), C_4H (Sakai et al. 2013), cyclic- C_3H_2 (Yoshida et al. 2015), and HC_5N (Takano et al. 1998, Taniguchi et al. 2016b) and can be discussed in terms of their respective formation pathways and some exchange reactions after formation.

The ^{13}C isotope anomaly of HC_3N in the starless cloud Taurus Molecular Cloud-1 Cyanopolyne Peak (hereafter referred to as TMC-1 CP) was investigated by Takano et al. (1998). The column densities of H^{13}CCCN , HC^{13}CCN , and HCC^{13}CN were reported to be $(2.0 \pm 0.2) \times 10^{12}$, $(2.1 \pm 0.2) \times 10^{12}$, and $(2.9 \pm 0.3) \times 10^{12} \text{ cm}^{-2}$, respectively, where the errors denote one standard deviation. Essentially, these abundance ratios reduce to 1.0:1.0:1.4 for $[\text{H}^{13}\text{CCCN}]:[\text{HC}^{13}\text{CCN}]:[\text{HCC}^{13}\text{CN}]$. On the basis of these ratios, Takano et al. (1998) pointed out that the reaction of $\text{C}_2\text{H}_2 + \text{CN}$ (Herbst & Leung 1990, Fukuzawa & Osamura 1997, Woon & Herbst 1997) is the most important pathway because the abundances of $[\text{H}^{13}\text{CCCN}]$ and $[\text{HC}^{13}\text{CCN}]$ should be equal to each other if the triple bond of C_2H_2 is conserved without breaking in the reaction. In addition, the reactions of $\text{C}_2\text{H}_2^+ + \text{HCN}$ (Huntress 1977, Schiff & Bohme 1979) and $\text{C}_2\text{H}_2 + \text{HCNH}^+$ (Mitchell et al. 1979) can also contribute to HC_3N production. Thus, it was suggested that HC_3N can be produced by reactions *via* C_2H_2 or C_2H_2^+ having two equivalent carbon atoms.

This pioneering result opened a new avenue for studying microscopic chemical processes in interstellar clouds through observations of ^{13}C isotopic species. However, the above argument is

based on the equal abundances of H^{13}CCCN and HC^{13}CCN . Although the abundances of the two species are similar to each other in TMC-1 CP, their ratio still has a mutual error of 14% in one standard deviation as the $J = 4-3$ rotational lines reported by Takano et al. (1998) have a signal-to-noise (S/N) ratio of 27 at most. The lines of the ^{13}C species of HC_3N in L1527 were recently observed by Taniguchi et al. (2016a), in which the abundance ratios of the three ^{13}C isotopic species of HC_3N were reported to be $0.9 \pm 0.2 : 1.00 : 1.29 \pm 0.19$ (one standard deviation) for $[\text{H}^{13}\text{CCCN}]:[\text{HC}^{13}\text{CCN}]:[\text{HCC}^{13}\text{CN}]$ based on the $J = 9-8$ and $10-9$ rotational lines having an S/N ratio of 11 at most. This observational result in L1527 implies equal abundances of H^{13}CCCN and HC^{13}CCN , but the ratios have large errors. It is therefore important to confirm the equal abundances of these two species as precisely as possible in order to stringently constrain the formation processes. Furthermore, the possible contribution of reactions exchanging the position of the ^{13}C atom within a molecule has been proposed for other carbon-chain molecules (Sakai et al. 2010b; Furuya et al. 2011), which is a possibility that needs to be examined carefully.

With these issues in mind, we observed the rotational transitions of the normal and isotopic species of HC_3N in order to precisely derive the isotopic abundance ratios in the low-mass star-forming region L1527, where HC_3N has been found to be abundant (Sakai et al. 2009b). The rotational spectral lines of DCCCN , HCCC^{15}N , and $\text{H}^{13}\text{CCCCCN}$ were also observed simultaneously. We discuss HC_3N production schemes in L1527 using these observational results.

2. OBSERVATIONS

2.1. Observations with the Green Bank 100 m Telescope

The $J = 5-4$ rotational lines of the three ^{13}C isotopic species and the normal species of HC_3N in the 42.2–45.5 GHz region listed in Table 1 were observed simultaneously using the Robert C. Byrd Green Bank Telescope (GBT) of the National Radio Astronomy Observatory¹ from March to October 2015. We observed the IRAS 04368+2557 position in L1527: $(\alpha 2000.0, \delta 2000.0) = (04^{\text{h}} 39^{\text{m}} 53^{\text{s}}.89, 26^{\circ} 03' 11.0'')$ (Sakai et al. 2008). The dual polarization Q-band receiver, whose instantaneous bandwidth is 4 GHz, was used. The system temperature during the observations ranged from 70 to 100 K depending on the elevation angle of the telescope and weather conditions. The main-beam efficiency is 0.83 and 0.81 in the 42.2 and 44.1–45.5 GHz regions, respectively (GBT Support Staff 2014). The half-power beam width (HPBW) of the telescope is $16.6''$ at 45.5 GHz. The pointing of the telescope was checked by observing the nearby continuum sources,

¹ The National Radio Astronomy Observatory is a facility of the National Science Foundation operated under cooperative agreement by Associated Universities, Inc.

J0336+3218 and J0319+4130, every 1.5 h, leading to a pointing accuracy of 5". The VErsatile GBT Astronomical Spectrometer (VEGAS) was used as a backend in the 23.44-MHz bandwidth and 1.4-kHz resolution mode, corresponding to a velocity resolution of 0.15–0.16 km/s by 16-channel smoothing. A frequency-switching mode with a frequency offset of ± 2.5 MHz was employed for the observations. The intensity scale was calibrated by noise injection. To obtain the final spectra, the right- and left-circular polarization spectra were averaged.

2.2. Observations with the Nobeyama 45 m telescope

Observations in the 81.5–109.2 GHz region were carried out in 2008–2010 using the Nobeyama Radio Observatory (NRO) 45 m telescope,² where the 88.2–109.2 GHz region was observed as part of the Nobeyama 45 m Telescope Legacy Project. We observed the same position observed in the GBT measurements above. The dual-polarization side-band separating SIS mixer receivers T100V/H were used in the 88.2–91.0 and 109.2 GHz regions in which the spectra obtained using T100V and T100H were averaged. For observations in the 81.5 GHz region, only the T100V receiver was used. The main-beam efficiency is 0.49 and 0.42 in the 81.5 and 88.2–109.2 GHz regions, respectively. The beam size of the telescope is 19.6", 18.1", 17.7", and 15.5" at 81.5, 88.2, 91.0, and 109.2 GHz, respectively. The telescope pointing was checked by observing the nearby SiO maser ($\nu = 1, J = 1-0$) in NML Tau every 1.5 h. The typical pointing accuracy was a few arc-seconds. A position switching mode with the off position taken at $\Delta\alpha = 30'$ and $\Delta\delta = 30'$ was employed for the observations. A set of acousto-optical spectrometers (AOSs) was used for the backend. The bandwidth and the frequency resolution of each wide-band AOS are 250 MHz and 250 kHz, respectively, and those of each high-resolution AOS are 40 MHz and 37 kHz, respectively. The frequency resolutions of the wide-band and high-resolution AOSs correspond to velocity resolutions of 0.92 km s^{-1} and 0.14 km s^{-1} , respectively, at 81.5 GHz. The intensity scale was calibrated using a chopper wheel method.

3. RESULTS

3.1. Column Density

The observed lines of the isotopic and normal species of HC₃N are shown in Figures 1–3, and their line parameters obtained from Gaussian fitting are listed in Table 1. Due to the high sensitivity of the GBT, S/N ratios as high as 35–44 were achieved for the $J = 5-4$ lines of the three

² The 45 m telescope is operated by the Nobeyama Radio Observatory, a branch of National Astronomical Observatory of Japan.

^{13}C isotopic species, which are less abundant and consequently have weak lines ($T_{\text{MB}} \leq 0.1$ K). Two weak satellite hyperfine components of the $J = 5-4$ transition for the normal species were also detected with $S/N = 53$ and 54 , respectively.

As shown in Figure 1, the $J = 5-4$ line for HCC^{13}CN is clearly brighter than those for H^{13}CCCN and HC^{13}CCN . This trend can be confirmed through a comparison of the integrated intensities (Table 1). A similar trend is also seen in the $J = 10-9$ lines, although the S/N ratio is not as high as for the $J = 5-4$ lines. Thus, a $^{12}\text{C}/^{13}\text{C}$ anomaly is evident among the three carbon atoms of HC_3N in L1527.

To enable quantitative analyses of the $^{12}\text{C}/^{13}\text{C}$ anomaly, the column density and the excitation temperature of each ^{13}C isotopic species of HC_3N are determined through least-square fitting of the integrated intensities of the observed lines under the assumption of local thermodynamic equilibrium (LTE). The $J = 9-8$ lines of HC^{13}CCN and HCC^{13}CN are half-weighted in the least-square fitting because they have lower S/N ratios and lower frequency resolution. Here, the source coupling factor is assumed to be unity, which is justified because the C_4H and CCH emitting regions of $30-40''$ (Sakai et al. 2008, 2010a) are larger than the beam sizes of the Green Bank and NRO observations. Partition functions are numerically calculated by summing over rotational energy levels up to $J = 60$. The dipole moment of $\mu = 3.73$ D for the ground vibrational state of HCCCN (DeLeon & Muentner 1985) is also used for all of the ^{13}C isotopic species. Results of the least-squares fit are summarized in Table 2. The excitation temperatures obtained for the three species H^{13}CCCN , HC^{13}CCN , and HCC^{13}CN are similar. The maximum optical depth is 0.01 for the $J = 5-4$ lines of HCC^{13}CN .

In this study, the effects of the hyperfine splitting owing to the ^{14}N nucleus ($I = 1$) are treated as follows. We use unsplitted intensities without hyperfine structures in the evaluation of column densities and excitation temperatures. The observed lines of HC_3N and its isotopic species (except for HCCC^{15}N) consist of the three main hyperfine components ($\Delta F = +1$) in the $J = (J'' + 1) - J''$ rotational transition, which are blended together. In addition, the two satellite components ($\Delta F = 0$) appear at both sides of the main components. As the satellite components are much weaker than the main components, they can be detected only for the normal species. However, their contributions need to be considered in order to evaluate the unsplitted intensity without the hyperfine structure. The intensities of the three strong hyperfine components constitute 97.3, 99.2, 99.3, and 99.5% of the unsplitted intensities of the $J = 5-4$, $9-8$, $10-9$, and $12-11$ transitions, respectively (Townes & Schawlow 1955). To obtain column densities and excitation temperatures, the integrated intensities corrected by these factors are used and are listed as W_{all} in Table 1.

We accurately derive the abundance ratios among the isotopic species from the $J = 5-4$

transitions observed at high S/N ratios by using the common excitation temperature for all isotopic species. Here we assume no anomalous excitation among the isotopic species. The HCCCN lines are not appropriate for obtaining a best estimate of the common excitation temperature because of the high opacity; therefore, we employ the HCC¹³CN lines, which are the brightest among the three ¹³C species. As mentioned above, the column density and excitation temperature of HCC¹³CN are obtained to be $(3.93 \pm 0.17) \times 10^{11} \text{ cm}^{-2}$ and $12.1 \pm 0.7 \text{ K}$, respectively, where the errors denote one standard deviation (Table 2). The root-mean-square (rms) residual of the fit for the three HCC¹³CN lines is 3.1 mK, which is roughly comparable with the noise level (rms) of the spectra (see Table 1). Thus, we use the excitation temperature of 12.1 K for all isotopic species as the common excitation temperature. The derived column densities are summarized in Table 3. The error of each column density, except for HCC¹³CN, is evaluated from the error of the temperature of HCC¹³CN and that of the integrated line intensity of each species, as each column density is derived by relative comparison with the intensity of HCC¹³CN.

To evaluate the column densities of HCCCN and DCCCN, Sakai et al. (2009b) considered different excitation temperatures for the following cases: the “low” J transition case for the $J = 5-4$ and $10-9$ lines, and the “high” J transition case for the $J = 10-9$ and $17-16$ lines. They reported excitation temperatures of 9.7 K and 16.9 K, respectively, for the low and high J transition cases. The temperature of $12.1 \pm 0.7 \text{ K}$ of HCC¹³CN obtained in the present observations is just between these and is close to that of the “low” J transition case.

The column density of HCCCN is derived from the ratio of the integrated intensities between HCCCN and HCC¹³CN using the common excitation temperature mentioned above. However, the main hyperfine components of HCCCN are not suitable for this purpose because the optical depth is moderate (0.44) for the $J = 5-4$ line. Hence, we employ the integrated intensities of the two weak $F = 5-5$ and $4-4$ components of $J = 5-4$ in order to derive the unsplitted intensity summing up all of the hyperfine components in the case of the optically thin condition. The unsplitted integrated intensity is thus evaluated to be $4.364 \pm 0.050 \text{ K km s}^{-1}$, as listed in Table 1. On the other hand, the integrated intensity of HCC¹³CN is $0.0676 \pm 0.0008 \text{ K km s}^{-1}$. The rotational constants of HCCCN (4549 MHz) and HCC¹³CN (4530 MHz) are very close to each other (Thorwirth *et al.* 2001), and hence the partition functions are comparable with each other for both species. Thus, the column density of HCCCN is estimated to be $2.52 \times 10^{13} \text{ cm}^{-2}$ from the column density of HCC¹³CN and the ratio of the integrated intensities between HCCCN and HCC¹³CN. This column density is consistent with that of $(1.9 \pm 0.5) \times 10^{13} \text{ cm}^{-2}$ obtained by the fitting of the three transitions of $J = 5-4$, $10-9$, and $12-11$ (Table 2), and agrees with that of $(2.7 \pm 0.2) \times 10^{13} \text{ cm}^{-2}$ reported by Sakai et al. (2009b) for the “low” J transition case.

3.2. Isotopic Ratios in HC_3N

In this study, the column densities of the normal and isotopic species are derived with high precision from the intensities of the $J = 5-4$ transitions (Figure 1), which were measured with very high S/N ratios. We derive the ^{13}C abundance ratios as $[H^{13}CCCN]:[HC^{13}CCN]:[HCC^{13}CN]:[HCCCN] = 1.00:1.01 \pm 0.02:1.35 \pm 0.03:86.4 \pm 1.6$ in L1527, in which the errors denote one standard deviation derived from the rms noise of the spectra. Our observational results are mostly consistent with those of Taniguchi et al. (2016a), but our results are much more precise. In particular, the equality of the $H^{13}CCCN$ and $HC^{13}CCN$ abundances is now confirmed within the one-sigma confidence level of 2%. This is much more stringent than the result for TMC-1 CP (Takano et al. 1998). Furthermore, the $[H^{13}CCCN]:[HC^{13}CCN]:[HCC^{13}CN]$ ratios obtained for L1527 are very close to those in TMC-1 CP.

In addition, The column densities of $DCCCN$ and $HCCC^{15}N$ are also derived from the intensities of the $J = 5-4$ transitions using the method used for the ^{13}C species. Then the ratios of $[HCCCN]/[HCCC^{15}N]$ and $[DCCCN]/[HCCCN]$ are obtained to be 338 ± 12 and 0.0370 ± 0.0007 (1σ), respectively.

In general, calibration errors, weather conditions, and pointing differences can affect integrated intensities; however, these effects were minimized in this study because all of the GBT data were obtained simultaneously. Moreover, none of the assumptions regarding the LTE condition, the excitation temperature, or the beam filling factor cause systematic errors in the obtained ratios because they are nearly canceled out in taking the ratios. The results are summarized in Table 3.

3.3. Isotopic Ratio in HC_5N

The $J = 17-16$ transition of $H^{13}CCCCCN$ was observed at 44.09 GHz using the GBT, as shown in Figure 3. The normal species of HC_5N was observed in L1527 by Sakai et al. (2009b), and the column density and the excitation temperature are derived to be $(6.8 \pm 1.4) \times 10^{12} \text{ cm}^{-2}$ and $14.7 \pm 5.3 \text{ K}$, respectively, by using the $J = 16-15$, $17-16$, and $32-31$ lines. The column density of $H^{13}CCCCCN$ is calculated to be $(7.2 \pm 0.8) \times 10^{10} \text{ cm}^{-2}$ under the assumption of LTE at the excitation temperature of 14.7 K. Based on this, the isotopic ratio of $[HCCCCCN]/[H^{13}CCCCCN]$ is evaluated to be 94 ± 29 (1σ), which is consistent with the $[HCCCN]/[H^{13}CCCN]$ ratio of 86.4 ± 2.2 and the $[HCCCN]/[HC^{13}CCN]$ ratio of 85.4 ± 2.4 listed in Table 4.

4. DISCUSSION

4.1. Anomaly of the $^{12}\text{C}/^{13}\text{C}$ ratios in HC_3N

In this study, we unambiguously find that the $^{12}\text{C}/^{13}\text{C}$ ratios for the three carbon-atoms of HC_3N vary in L1527. A similar anomaly is reported for HC_3N , CCS , C_3S , CCH , and C_4H in TMC-1 CP and for CCH and $c\text{-C}_3\text{H}_2$ in L1527. Two possibilities are proposed as the origin of this anomaly. One is that the anomaly reflects a production pathway of molecules, as discussed in previous papers (Takano et al. 1998; Sakai et al. 2007, 2010b, 2013; Yoshida et al. 2015). If a parent molecule has equivalent carbon atoms by symmetry, it cannot produce different $^{12}\text{C}/^{13}\text{C}$ ratios in a particular part of a product molecule. For instance, the different $^{12}\text{C}/^{13}\text{C}$ ratios for the two carbon atoms in CCH would exclude formation from the electron recombination reaction of C_2H_2^+ , which has equivalent carbon atoms, as a main formation pathway. Another possibility is that an exchange reaction is stabilizing the energetically stable isotopic species, for instance:



Because C^{13}CH is more energetically stable than ${}^{13}\text{CCH}$ by 8.1 K (Sakai et al. 2010b), the $\text{C}^{13}\text{CH}/{}^{13}\text{CCH}$ ratio would be expected to be enhanced. Such exchange reactions after the formation of the molecules could contribute to the anomaly.

In the case of HC_3N , Takano et al. (1998) proposed the former possibility to explain the isotope anomaly in TMC-1 CP. HC_3N is primarily formed through the reaction of $\text{C}_2\text{H}_2 + \text{CN}$, and the $^{12}\text{C}/^{13}\text{C}$ ratios of C_2H_2 and CN can differ as a result of their different formation histories and ^{13}C fractionation processes. For instance, the $^{12}\text{C}/^{13}\text{C}$ ratio in CN can be **lower** for the following fractionation reaction:



which is exothermic by 31.1 K (Roueff et al. 2015). On the other hand, a similar reaction does not occur for C_2H_2 . If the CN part of HC_3N does come from the CN molecule, the $^{12}\text{C}/^{13}\text{C}$ ratio for the nitrile carbon could be lower than those for the other two carbon atoms coming from C_2H_2 . This scheme is also possible in L1527 if HC_3N was produced in a cold starless phase before the onset of star formation.

On the other hand, the second possibility does not significantly contribute to the $^{12}\text{C}/^{13}\text{C}$ anomaly in HC_3N . Because HC_3N is a closed-shell molecule, exchange reactions similar to Equation (2) seem unlikely. This conclusion can be further confirmed by the following consideration. The zero-point vibrational energies of H^{13}CCCN , HC^{13}CCN , and HCC^{13}CN are lower than that of the normal species by 48.9, 56.8, and 63.8 K, respectively (Takano et al. 1998). If the exchange reactions are responsible for the isotopic ratios, the abundances of H^{13}CCCN ,

HC^{13}CCN , and HCC^{13}CN should increase in that order. However, the measured abundance ratios, that is $[\text{H}^{13}\text{CCCN}] \approx [\text{HC}^{13}\text{CCN}] < [\text{HCC}^{13}\text{CN}]$, differ from this prediction. Indeed, the equilibrium ratio is 0.5:1.0:2.0 at 10 K and 0.7:1.0:1.3 at 25 K if the $^{12}\text{C}/^{13}\text{C}$ anomaly is caused by some thermal isotope exchange reactions. In the range of the gas kinetic temperature (10 K for the cold starless phase and 25 K for the WCCC condition), the observed ratios cannot be explained by the thermal equilibrium. Therefore, the anomaly of the $^{12}\text{C}/^{13}\text{C}$ ratios of HC_3N in L1527 likely reflects the HC_3N formation mechanisms.

The $[\text{H}^{13}\text{CCCN}]:[\text{HC}^{13}\text{CCN}]:[\text{HCC}^{13}\text{CN}]$ ratios in L1527 are very similar to those of TMC-1 CP. This suggests that reaction (2) followed by the reaction $\text{C}_2\text{H}_2 + \text{CN}$ could be at work in L1527 as well as in TMC-1 CP. Hence, it is likely that the HC_3N observed in L1527 was produced in a similar low temperature condition to that in TMC-1 CP, i.e., it could be a remnant of a cold starless phase of the cloud and therefore produced before the start of WCCC. However, it should be noted that not all of the HC_3N in L1527 would be a remnant of this phase. Multi-transition observations of the $J = 5-4$, $10-9$, and $17-16$ transitions of HC_3N reported by Sakai et al. (2009b) suggest that two HC_3N components having high (16.9 K) and low (9.7 K) temperatures exist for HC_3N in this cloud. In contrast to TMC-1 CP, the high temperature component in L1527 would originate from the WCCC effect in the vicinity of the protostar. The excitation temperature of 12.1 K of HC_3N obtained in this work using the $J = 5-4$, $9-8$, and $10-9$ transitions is close to that of the low temperature component, and the ratios are determined by using the $J = 5-4$ transition. Hence, the present ratios are likely to be characteristic of the low temperature component. The ratios of the high temperature component are also interesting, and observations of the ^{13}C species of HC_3N in high J transitions in L1527 are awaited.

4.2. Dilution of ^{13}C in HC_3N

It has been reported that the ^{13}C atom is diluted in carbon-chain molecules. Here, we examine the $^{12}\text{C}/^{13}\text{C}$ ratios of HC_3N in L1527 in this context. The $^{12}\text{C}/^{13}\text{C}$ ratios for H^{13}CCCN , HC^{13}CCN , and HCC^{13}CN are determined to be 86.4 ± 2.2 , 85.4 ± 2.4 , and 64.2 ± 1.5 , respectively. The $\text{HCCCN}/\text{HCC}^{13}\text{CN}$ ratio (64) is almost comparable to the elemental ratio of 60–70 in the local interstellar medium (Lucas & Liszt 1998; Milam et al. 2005). On the other hand, the $\text{HCCCN}/\text{H}^{13}\text{CCCN}$ and $\text{HCCCN}/\text{HC}^{13}\text{CCN}$ ratios are significantly higher than the elemental ratio. The average $^{12}\text{C}/^{13}\text{C}$ ratio of HC_3N , defined as

$$R_{av}(\text{HC}_3\text{N}) = \frac{3 [\text{HC}_3\text{N}]}{[\text{H}^{13}\text{CCCN}] + [\text{HC}^{13}\text{CCN}] + [\text{HCC}^{13}\text{CN}]}$$

is 77 ± 4 , which is slightly higher than the elemental ratio. This means that ^{13}C is likely diluted in HC_3N . The average $^{12}\text{C}/^{13}\text{C}$ ratios for CCH and *c*- C_3H_3 are reported to be > 200 (Sakai et al.

2010b) and 150 ± 30 (Yoshida et al. 2015), and hence, the dilution in HC_3N is not as significant as in CCH or $c\text{-C}_3\text{H}_2$. This trend can also be seen in TMC-1 CP. According to Takano et al. (1998), the average $^{12}\text{C}/^{13}\text{C}$ ratio in TMC-1 CP is 69, which is almost within the range of the elemental ratio. By contrast, the average $^{12}\text{C}/^{13}\text{C}$ ratios for CCS, CCH, and C_4H in TMC-1 CP are 87 (Sakai et al. 2013), > 200 , and 105 (Sakai et al. 2013), respectively. Hence, the ^{13}C dilution is less significant in HC_3N than in the other carbon-chain molecules mentioned above. The similarity between L1527 and TMC-1 CP in terms of ^{13}C dilution in HC_3N further supports the assumption that the HC_3N observed in L1527 was mainly formed under a similar condition to that in TMC-1 CP (i.e., a low temperature condition).

The average $^{12}\text{C}/^{13}\text{C}$ ratios for the longer cyanopolyynes HC_5N and HC_7N in TMC-1 CP are 94 ± 6 (Taniguchi et al. 2016b) and > 52 (Langston & Turner 2007), respectively. These ratios are not **very** different from the average $^{12}\text{C}/^{13}\text{C}$ ratio in HC_3N . This trend can be seen in L1527. Our observations of $\text{H}^{13}\text{CCCCCN}$ in L1527 using GBT reveal a $^{12}\text{C}/^{13}\text{C}$ ratio of 94 ± 29 , which is comparable to the average $^{12}\text{C}/^{13}\text{C}$ ratio in HC_3N .

Above all, the dilution of ^{13}C in cyanopolyynes is less significant than in other series of carbon-chain molecules, e.g., CCH (Sakai et al. 2010b), in both TMC-1 CP and L1527. This contradicts the results of the chemical model simulation by Furuya et al. (2011), which predict nearly the same dilution both for HC_3N and CCH. This result implies that the formation region of HC_3N (and probably HC_5N) is different from that for CCH and $c\text{-C}_3\text{H}_2$. Indeed, it is well known that different series of carbon-chain molecules (i.e., C_nH , C_nS , and HC_nN) show different distributions in TMC-1 CP (Olano et al. 1988, Hirahara et al. 1992, Langer et al. 1995, Pratap et al. 1997, Dickens et al. 2001). It is important to delineate distributions of HC_3N in the protostellar core of L1527 and to compare these with the CCH distribution (Sakai et al. 2010a).

4.3. Isotopic Fractionation of ^{15}N and D in HC_3N

The $[\text{HCC}^{13}\text{CN}]/[\text{HCCC}^{15}\text{N}]$ ratio in L1527 is found to be 5.26 ± 0.19 (1σ), resulting in a $[\text{HCCCN}]/[\text{HCCC}^{15}\text{N}]$ ratio of 338 ± 12 . This is the first observation of the $^{14}\text{N}/^{15}\text{N}$ ratio of this molecule, and is close to the ratio of $[\text{H}^{13}\text{CN}]/[\text{HC}^{15}\text{N}] = 5.56 \pm 0.92$ in TMC-1 CP reported by Ikeda et al. (2002).

Using the Genesis solar wind sampling measurements, the $^{14}\text{N}/^{15}\text{N}$ ratio was determined to be 441 ± 6 (Marty et al. 2011), which is considered to be indicative of the composition of the so-called “proto-solar nebula” (PSN), from which our Sun was formed. In molecular clouds, the following $^{14}\text{N}/^{15}\text{N}$ ratios were measured from abundant N-bearing species. Observations of NH_3 reveal comparable ratios to those found in the PSN (e.g., Gerin et al. 2009, Lis et al. 2010, Daniel

et al. 2013), while N_2H^+ shows a ratio of $\sim 1000 \pm 200$ in the prestellar core L1544 (e.g., Bizzocchi et al. 2013). HCN and HNC have lower ratios: 140–360 (Hily-Blant et al. 2013), 160–290 (Wampfler et al. 2014), and 237 (–21, +27) (Lucas & List 1998). Observations of CN and HCN reveal that the ratio in the interstellar matter surrounding our Sun is as low as 290 ± 40 (Adande & Ziurys 2012). The $^{14}\text{N}/^{15}\text{N}$ ratio obtained from HC_3N in this study is similar to the ratios obtained for CN, HCN and HNC, which commonly have a nitrile.

The ratio of $[\text{HCCCN}]/[\text{DCCCN}]$ in L1527 is obtained to be 0.0370 ± 0.0010 (1σ), which agrees with the previously observed ratio of 0.031 ± 0.011 within the given error range (Sakai et al. 2009b). The ratio is higher by a factor of 2 than the ratio reported for TMC-1 CP (Turner 2001) and is roughly half of the ratio in the carbon-chain-rich prestellar core L1544 (Howe et al. 1994).

5. SUMMARY

1. The rotational transitions of the ^{13}C , ^{15}N , and D isotopic species and the normal species of HC_3N in the low-mass star-forming region L1527 were observed using the GBT and the Nobeyama 45 m telescope. In particular, the $J = 5-4$ lines of the three ^{13}C isotopic species were observed with high S/N ratios.
2. The ^{13}C isotopic ratios (fractionation) of HC_3N are accurately determined to be $[\text{H}^{13}\text{CCCN}]:[\text{HC}^{13}\text{CCN}]:[\text{HCC}^{13}\text{CN}]:[\text{HCCCN}] = 1.00:1.01 \pm 0.02:1.35 \pm 0.03:86.4 \pm 1.6$ (1σ). Based on a consideration of the zero-point energies of each isotopic species, these ratios cannot be explained as the results of carbon isotope exchange reactions after the formation of HC_3N . The ratios obtained for L1527 are very similar to those reported for the starless cloud TMC-1 CP, and it is likely that the HC_3N in L1527 is a remnant of a cold starless phase of this cloud.
3. The column densities of H^{13}CCCN and HC^{13}CCN in L1527 are found to be close to each other. Hence, the equality of the $^{12}\text{C}/^{13}\text{C}$ ratio for these two ^{13}C species is established unambiguously. This result puts a stringent constraint in the production pathway of HC_3N and strongly supports the production scheme of HC_3N *via* C_2H_2 and C_2H_2^+ .
4. The ratios of $[\text{HCCCN}]/[\text{DCCCN}]$ and $[\text{HCCCN}]/[\text{HCCC}^{15}\text{N}]$ in L1527 are precisely obtained as 0.0370 ± 0.0007 and 338 ± 12 , respectively. The ratio of $[\text{HCCCN}]/[\text{DCCCN}]$ is consistent with the previously reported ratio. On the other hand, the ratio of $^{14}\text{N}/^{15}\text{N}$ *via* HC_3N is likely lower than that of the proto-solar nebula.

Acknowledgment

We thank the staff at the Nobeyama Radio Observatory and the National Radio Astronomy

Observatory for help with the observations. We thank Dr. David Frayer for his help in the observations at the GBT. M.A. thanks Grant-in-Aid for Scientific Research on Innovative Areas (Grant No. 25108002), Grant-in-Aid for Scientific Research (C) (Grant No. 15K05395), and the Institute for Quantum Chemical Exploration.

REFERENCES

- Adande, G. R. & Ziurys, L. M. 2012, *ApJ*, 744, 194 DOI: 10.1088/0004-637X/744/2/194
- Aikawa, Y., Ohashi, N., Inutsuka, S., Herbst, E., & Takakuwa, S. 2001, *ApJ*, 552, 639 DOI: 10.1086/320551
- Aikawa, Y., Wakelam, V., Garrod, R. T., & Herbst, E. 2008, *ApJ*, 674, 984 DOI: 10.1086/524096
- Benson, P. J., Caselli, P., & Myers, P. C. 1998, *ApJ*, 506, 743 DOI: 10.1086/306276
- Bizzocchi, L., Caselli, P., Leonardo, E., & Dore, L. 2013, *A&A*, 555, 109 DOI: 10.1051/0004-6361/201321276
- Bizzocchi, L., Degli Esposti, C., & Botschwina, P. 2004, *J. Mol. Spec.*, 225, 145 DOI:10.1016/j.jms.2004.02.019
- Creswell, R. A., Winnewisser, G., & Gerry, M. C. L. 1977, *J. Mol. Spec.*, 65, 420 DOI: 10.1016/0022-2852(77)90281-8
- Coveliers, B., Ahmed, W. K., Fayt, A., & Maki, A. G. 1990, *J. Mol. Spec.*, 142, 148 DOI: 10.1016/0022-2852(90)90298-5
- Daniel, F., Gérin, M., Roueff, E., et al. 2013, *A&A*, 560, 3 DOI: 10.1051/0004-6361/201321939
- DeLeon, R. L. & Muenter J. S. 1985, *J. Chem. Phys.*, 82, 1702 DOI: 10.1063/1.4484
- Dickens, J. E., Langer, W. D., & Velusamy, T. 2001, *ApJ*, 558, 693. DOI: 10.1086/322292
- Fukuzawa, K. & Osamura, Y. 1997, *ApJ*, 489, 113
- Furuya, K., Aikawa, Y., Sakai, N., & Yamamoto, S. 2011, *ApJ*, 731, 38 DOI: 10.1088/0004-637X/731/1/38
- GBT Support Staff, The Proposer's Guide for the Green Bank Telescope (West Virginia, National Radio Astronomy Observatory), July 9, 2014, Semester 15A <https://science.nrao.edu/facilities/gbt>
- Gerin, M., Marcelino, N., Biver, N., et al. 2009, *A&A*, 498, L9 DOI: 10.1051/0004-6361/200911759
- Hassel, G. E., Herbst, E., & Garrod, R. T. 2008, *ApJ*, 681, 1385 DOI: 10.1086/588185
- Herbst, E. & Leung, C. M. 1990, *A&A*, 233, 177
- Hily-Blant, P., Bonal, L., Faure, A., & Quirico, E. 2013, *Icar*, 223, 582 DOI: 10.1016/j.icarus.2012.12.015

- Hirahara, Y., Suzuki, H., Yamamoto, S., et al. 1992, *ApJ*, 394, 539 DOI: 10.1086/171605
- Hirota, T., Ohishi, M., & Yamamoto, S. 2009, *ApJ*, 699, 585 DOI: 10.1088/0004-637X/699/1/585
- Howe, D. A., Millar, T. J., Schilke, P., & Walmsley, C. M. 1994, *MNRAS*, 267, 59 DOI: 10.1093/mnras/267.1.59
- Huntress, W. T. Jr. 1977, *ApJS*, 33, 495 DOI: 10.1086/190439
- Ikeda, M., Hirota, T., & Yamamoto, S. 2002, *ApJ*, 575, 250 DOI: 10.1086/341287
- Kahane, C., Gomez-Gonzalez, J., Cernicharo, J., & Guelin, M. 1988, *A&A*, 190, 167
- Kaiser, M. E., Wright, E. L., & Hawkins, I. 1991, *ApJ*, 379, 267 DOI: 10.1086/170500
- Lafferty, W. J. & Lovas, F. J. 1978, *J. Phys. Chem. Ref. Data*, 7, 441 DOI: 10.1063/1.555575
- Langer, W. D., Velusamy, T., Kuiper, T. B. H., et al., 1995, *ApJ*, 453, 293 DOI: 10.1086/176389
- Langston, G. & Turner, B. 2007, *ApJ*, 658, 455 DOI: 10.1086/511332
- Li, J., Shen, Z.-Q., Wang, J., et al. 2016, *ApJ*, 824, 136 DOI: 10.3847/0004-637X/824/2/136
- Lis, D. C., Wootten, A., Gerin, M., & Roueff, E. 2010, *ApJ*, 710, L49 DOI: 10.1088/2041-8205/710/1/L49
- Lucas, R. & Liszt, H. 1998, *A&A*, 337, 246
- Marka, C., Schreyer, K., Launhardt, R., Semenov, D. A., & Henning, T. H. 2012, *A&A*, 537, 4 DOI: 10.1051/0004-6361/201014375
- Marty, B., Chaussidon, M., Wiens, R. C., Jurewicz, A. J. G., & Burnett, D. S. 2011, *Science*, 332, 1533 DOI: 10.1126/science.1204656
- Mitchell, G. F., Huntress, W. T., Jr., & Prasad, S. S. 1979, *ApJ*, 233, 102 DOI: 10.1086/157370
- Microwave Spectroscopy, Townes, C. H., & Schawlow, A. L. 1955, Dover Publications, New York
- Müller, H. S. P., Schlöder, F., Stutzki, J., & Winnewisser, G. 2005, *J. Mol. Struct.*, 742, 215 DOI: 10.1016/j.molstruc.2005.01.027
- Müller, H. S. P., Thorwirth, S., Roth, D. A., & Winnewisser, G. 2001, *A&A*, 370, L49 DOI: 10.1051/0004-6361:20010367
- Olano, C. A., Walmsley, C. M., & Wilson, T. L. 1988, *A&A*, 196, 194
- Pratap, P., Dickens, J. E., Snell, R. L. et al. 1997, *ApJ*, 486, 862
- Rathborne, J. M., Lada, C. J., Muench, A. A., Alves, J. F., & Lombardi, M. 2008, *ApJS*, 174, 396 DOI: 10.1086/522889
- Roueff, E., Loison, J. C., & Hickson, K. M. 2015, *A&A*, 576, 99 DOI:10.1051/0004-6361/201425113
- Sakai, N., Ikeda, M., Morita, M., et al. 2007, *ApJ*, 663, 1174 DOI: 10.1086/518595
- Sakai, N., Sakai, T., Hirota, T., Burton, M., & Yamamoto, S. 2009a, *ApJ*, 697, 769 DOI:

10.1088/0004-637X/697/1/769

Sakai, N., Sakai, T., Hirota, T., & Yamamoto, S. 2009b, *ApJ*, 702, 1025 DOI: 10.1088/0004-637X/702/2/1025

Sakai, N., Sakai, T., Hirota, T., & Yamamoto, S. 2008, *ApJ*, 672, 371 DOI: 10.1086/523635

Sakai, N., Sakai, T., Hirota, T., & Yamamoto, S. 2010a, *ApJ*, 722, 1633 DOI: 10.1088/0004-637X/722/2/1633

Sakai, N., Saruwatari, O., Sakai, T., Takano, S., & Yamamoto, S. 2010b, *A&A*, 512, A31 DOI: 10.1051/0004-6361/200913098

Sakai, N., Takano, S., Sakai, T., et al. 2013, *JPCA*, 117, 9831 DOI: 10.1021/jp3127913

Sakai, N. & Yamamoto, S. 2013, *Chem. Rev.*, 113, 8981 DOI: 10.1021/cr4001308

Saleck, A. H., Simon, R., Winnewisser, G., & Wouterloot, J. G. A. 1994, *Can. J. of Phys.* 72, 747 DOI: 10.1139/p94-098

Schiff, H. I. & Bohme, D. K. 1979, *ApJ*, 232, 740 DOI: 10.1086/157334

Spahn, H., Müller, H. S. P., Giesen, T. F., et al. 2008, *Chem. Phys.*, 346, 132 DOI: 10.1016/j.chemphys.2007.12.018

Takano, S., Masuda, A., Hirahara, Y., et al. 1998, *A&A*, 329, 1156

Taniguchi, K., Ozeki, H., Saito, M., et al. 2016b, *ApJ*, 817, 147 DOI: 10.3847/0004-637X/817/2/147

Taniguchi, K., Saito, M., & Ozeki, H. 2016a, arXiv:1608.01702 [astro-ph.GA], *ApJ* in press

Thorwirth, S., Mueller, H. S. P., & Winnewisser, G., 2001, *PCCP*, 3, 1236 DOI:10.1039/B009743H

Turner, B. E. 2001, *ApJS*, 136, 579 DOI: 10.1086/322536

Wampfler, S. F., Jørgensen, J. K., Bizzarro, M., & Bisschop, S. E. 2014, *A&A*, 572, 24 DOI: 10.1051/0004-6361/201423773

Wannier, P. G. & Linke, R. A. 1978, *ApJ*, 226, 817 DOI: 10.1086/156661

Woon, D. E. & Herbst, E. 1997, *ApJ*, 477, 204

Yoshida, K., Sakai, N., Tokudome, T., et al. 2015, *ApJ*, 807, 66 DOI: 10.1088/0004-637X/807/1/66

Table 1. Molecular Lines Observed in L1527.

Transition	Species	Frequency ^a (GHz)	Telescope	T_{MB} (K)	$\Delta\nu$ ^b (km s ⁻¹)	W ^c (K km s ⁻¹)	W_{all} ^d (K km s ⁻¹)	rms in T_{MB} (mK)	V_{LSR} (km s ⁻¹)
$J = 5-4$	H ¹³ CCCN ^e	44.0841622 ^f	GBT	0.0703(5)	0.633(5)	0.0473(7)	0.0486(7)	1.6	5.9
	HC ¹³ CCN ^e	45.2973345 ^f	GBT	0.0745(6)	0.630(6)	0.0500(8)	0.0513(9)	2.1	5.9
	HCC ¹³ CN ^e	45.3017069 ^f	GBT	0.0937(5)	0.660(4)	0.0658(8)	0.0676(8)	2.2	5.9
	HCCCN ^e	45.4903138 ^f	GBT	3.275(13)	0.785(3)	2.738(23)	2.814(23)	2.6	5.9
	$F = 5-5$	45.4888386 ^g	GBT	0.1380(9)	0.394(3)	0.0579(8)	4.364(50) ^h	2.6	5.92
	$F = 4-4$	45.4921104 ^g	GBT	0.1415(6)	0.388(2)	0.0585(5)		2.6	5.91
	HCCC ¹⁵ N	44.1672678 ^f	GBT	0.0265(4)	0.444(8)	0.0125(4)	← ⁱ	2.1	5.94
DCCCN ^e	42.2155827 ^f	GBT	0.2007(14)	0.662(5)	0.1413(21)	0.1452(21)	2.0	5.9	
$J = 9-8$	HC ¹³ CCN ^e	81.5341106 ^f	NRO ^j	0.039(8)	1.00(25) ^j	0.041(10)	0.041(10)	9.1	6.0
	HCC ¹³ CN ^e	81.5419806 ^f	NRO ^j	0.046(7)	1.7(3) ^j	0.084(16)	0.085(16)	10.2	5.9
$J = 10-9$	H ¹³ CCCN ^e	88.166832 ^f	NRO ^k	0.083(8)	0.43(5)	0.038(8)	0.039(8)	14.4	6.1
	HC ¹³ CCN ^e	90.593059 ^f	NRO ^k	0.095(9)	0.53(5)	0.053(10)	0.054(10)	14.4	6.0
	HCC ¹³ CN ^e	90.601777 ^f	NRO ^k	0.120(7)	0.52(4)	0.066(8)	0.067(8)	14.5	5.9
	HCCCN ^e	90.979023 ^f	NRO ^k	4.115(18)	0.607(3)	2.660(25)	2.678(25)	18.1	6.0
$J = 12-11$	HCCCN ^e	109.1736340 ^f	NRO ^k	4.79(3)	0.622(5)	3.17(4)	3.19(4)	28.3	5.9
$J = 17-16$	H ¹³ CCCCCN ^e	44.0864313 ^f	GBT	0.0129(5)	0.472(22)	0.0065(3)	← ⁱ	2.1	5.89

Note. The numbers in parentheses are errors in units of the last significant digits.

^a Rest frequency.

^b FWHM obtained by Gaussian fit.

^c $W = \int T_{\text{MB}} d\nu$.

^d Estimated integrated intensities summing up all hyperfine components. For example, the relative intensities are $F = 5-5:6-5:5-4:4-3:4-4 = 0.0133:0.3939:0.3200:0.2593:0.0133$ for the $J = 5-4$ transitions (Townes & Schawlow 1955).

^e Blended lines of three hyperfine components $\Delta F = +1$ for the $J = (J''+1) - J''$ rotational transitions.

^f The Cologne Database for Molecular Spectroscopy (Müller et al. 2001, 2005). Laboratory data for HC₃N and DC₃N were reported by Thorwirth et al. (2001) and Spahn et al. (2008), respectively. For H¹³CCCCCN, the molecular constants come from Bizzocchi et al. (2004).

^g Lafferty & Lovas 1978.

^h The unsplitted integrated intensity estimated from $\Delta F = 0$ components summing up all the hyperfine components of the $J = 5-4$ transition in the case of the optically thin condition.

ⁱ W_{all} is equal to W because of no hyperfine splittings.

^j Wide band AOS: The line widths are overestimated.

^k High-resolution AOS.

Table 2. Column densities N and excitation temperatures T of the normal and ^{13}C isotopic species of HC_3N in L1527. ^a

Species	Lines used	N (cm^{-2}) ^b	T (K) ^b
H^{13}CCCN	$J = 5-4, 10-9$	2.8×10^{11}	10
HC^{13}CCN	$J = 5-4, 9-8,^c 10-9$	$(2.8 \pm 0.6) \times 10^{11}$	12 ± 3
HCC^{13}CN	$J = 5-4, 9-8,^c 10-9$	$(3.93 \pm 0.17) \times 10^{11}$	12.1 ± 0.7
HCCCN	$J = 5-4,^d 10-9, 12-11$	$(1.9 \pm 0.5) \times 10^{13}$	16 ± 4

^a The dipole moment $\mu = 3.73$ D (DeLeon & Muentner 1985) is used.

^b The errors are 1σ .

^c Half weighted in the least square fitting because of the lower S/N.

^d The integrated intensity of $W_{\text{all}} = 2.814(23)$ K km s⁻¹ in Table 1 is used.

Table 3. Column densities N and isotopic abundance ratios for HC_3N in L1527 derived from the integrated intensities W_{all} of the observed transitions by using the common excitation temperature of 12.1 K.

Species	$J = 5-4$			$J = 10-9$	
	N (cm^{-2})	Ratio ^a			Ratio ^a
		^{13}C	H	^{15}N	^{13}C
H^{13}CCCN	$(2.91 \pm 0.06) \times 10^{11}$ ^b	1.0		1.0	
HC^{13}CCN	$(2.95 \pm 0.07) \times 10^{11}$ ^b	1.01 ± 0.02		1.4 ± 0.4	
HCC^{13}CN	$(3.93 \pm 0.17) \times 10^{11}$ ^c	1.35 ± 0.03		1.7 ± 0.4	
HCCC^{15}N	$(7.5 \pm 0.3) \times 10^{10}$ ^b			1.0	
DCCCN	$(9.3 \pm 0.2) \times 10^{11}$ ^{b, d}		0.0370 ± 0.0007		
HCCCN	$(2.52 \pm 0.05) \times 10^{13}$ ^{b, e}	86.4 ± 1.6	1.0	338 ± 12	

Note. The column densities N and the isotopic abundance ratios are derived from W_{all} in Table 1.

^a The errors (1σ) come from only the errors of W_{all} in Table 1.

^b The error (1σ) is derived from both the error of the temperature of HCC^{13}CN and that of the integrated line intensity of each species. The former is canceled out by taking the ratios.

^c The error (1σ) is obtained by least square fitting of the line intensities of the $J = 5-4$, $9-8$, and $10-9$ transitions, as shown in Figure 1.

^d The dipole moment of DCCCN is $\mu = 3.74$ D (Coveliers et al. 1990), while that of the others are $\mu = 3.73$ D (DeLeon & Muentner 1985).

^e The integrated intensity W_{all} derived from the intensities of $F = 5-5$ and $4-4$ is used.

Table 4. The ^{13}C isotopic ratios of HC_3N and CCH in L1527 and TMC-1 CP.

Ratio	L1527	TMC-1 CP ^a
$[\text{HCCCN}]/[\text{H}^{13}\text{CCCN}]$	86.4 ± 1.6 ^b	79 ± 11 ^c
$[\text{HCCCN}]/[\text{HC}^{13}\text{CCN}]$	85.4 ± 1.7 ^b	75 ± 10 ^c
$[\text{HCCCN}]/[\text{HCC}^{13}\text{CN}]$	64.2 ± 1.1 ^b	55 ± 7 ^c
$[\text{CCH}]/[\text{C}^{13}\text{CH}]$	≥ 80 ^d	≥ 170 ^d
$[\text{CCH}]/[^{13}\text{CCH}]$	≥ 135 ^d	≥ 250 ^d

^a The cyanopolyne peak (CP).

^b The errors come from the errors of W_{all} in Table 1.

^c Takano et al. 1998. ^d Sakai et al. 2010b.

FIGURES

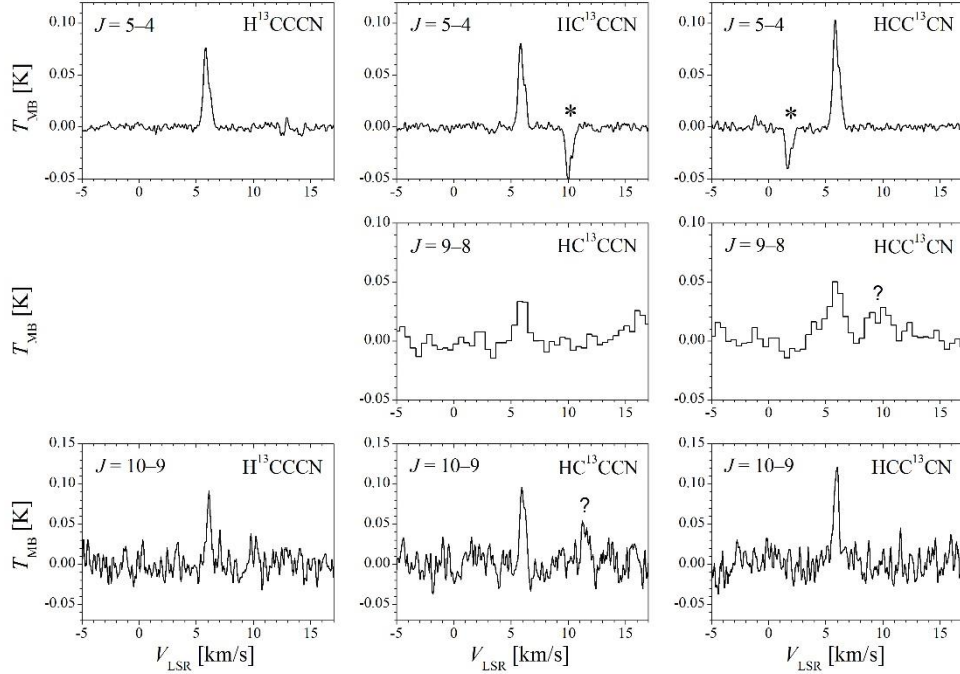


Figure 1. Observed lines of the $J = 5-4$, $9-8$, and $10-9$ transitions of the isotopic species H^{13}CCCN , HC^{13}CCN , and HCC^{13}CN in L1527. The $J = 5-4$ transitions were observed with the Green Bank 100 m telescope. The $J = 9-8$ and $10-9$ transitions were with the NRO 45 m telescope using the wide-band and high-resolution acousto-optical spectrometers, respectively. Negative features indicated by the asterisks are frequency switch artifacts of other lines. Features labeled by the question marks are artifacts.

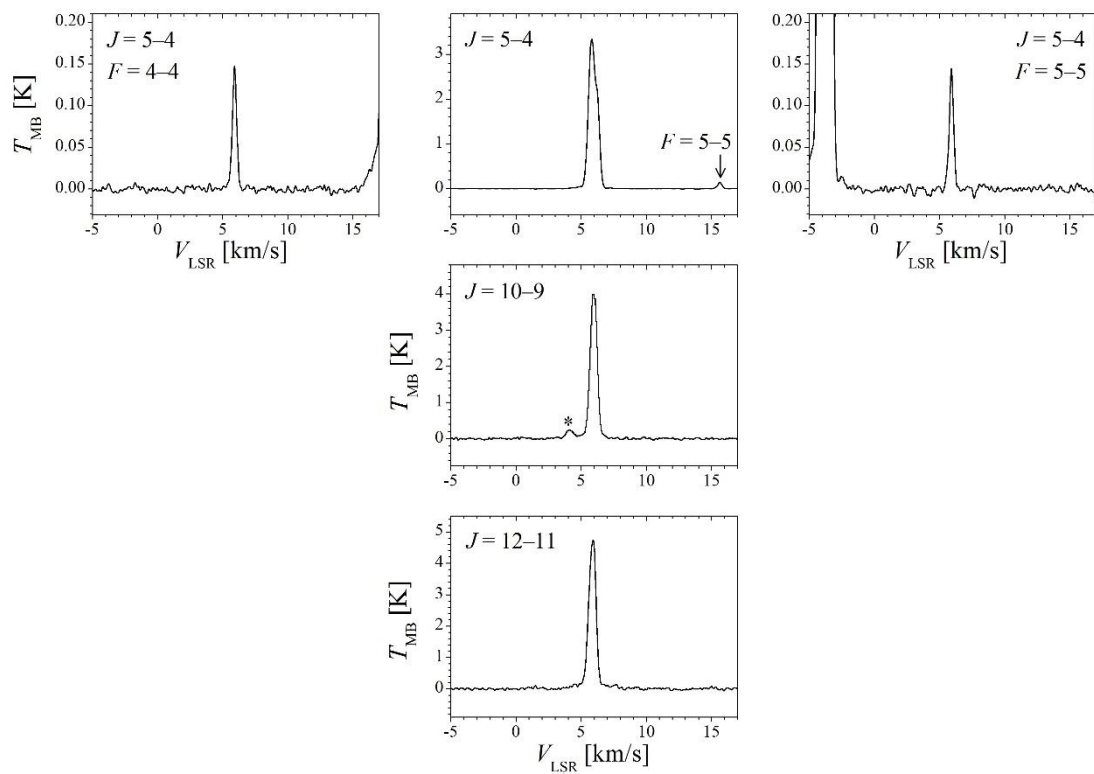


Figure 2. Observed lines of the $J = 5-4$, $10-9$, and $12-11$ transitions of the normal species HCCCN in L1527. The blended lines of the three strong hyperfine components are shown in the middle column. The small feature indicated by the asterisk is an image-side band artifact.

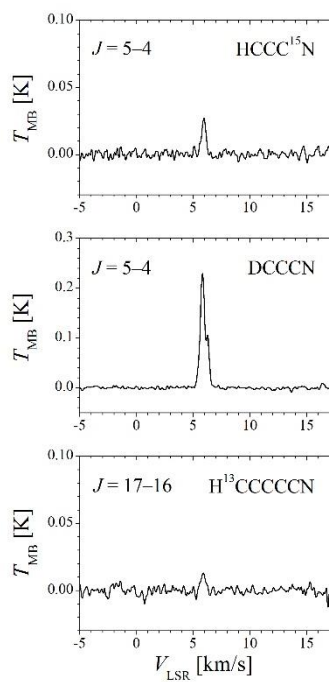


Figure 3. Observed lines of HCCC^{15}N , DCCCN , and $\text{H}^{13}\text{CCCCCN}$ in L1527.